Shielding Effectiveness of a Loaded Enclosure in the Non-Reverberant Range: Comparison of Simulation and Reverberation Chamber Measurements

Ali Ghaffarlouy Raef
School of Physics, Engineering and Technology
University of York
York, UK
ali.raef@york.ac.uk

Andrew C. Marvin
School of Physics, Engineering and Technology
University of York
York, UK
andy.marvin@york.ac.uk

Simon J. Bale
School of Physics, Engineering and Technology
University of York
York, UK
simon.bale@york.ac.uk

Martin P. Robinson
School of Physics, Engineering and Technology
University of York
York, UK
martin.robinson@york.ac.uk

John F. Dawson
School of Physics, Engineering and Technology
University of York
York, UK
John.dawson@york.ac.uk

Abstract— Measuring shielding effectiveness (SE) in the non-reverberant frequency range of an enclosure is challenging because the internal field is not statistically uniform and the results depend strongly on enclosure geometry, apertures, loading, and the measurement location. This paper presents a simulation based numerical approach that mimics a reverberation chamber (RC) based measurement without modelling the full chamber and stirrers.

A finite set of full-wave plane-wave illuminations is generated using angular sampling methods and combined using plane-wave superposition (PWS) approach to form an ensemble of realizations. Gauss-Legendre Quadrature (GLQ) and Lebedev methods are first compared, after which GLQ is adopted for the remainder of the study due to its accuracy and efficiency trade-off. Validation against RC measurements using point shielding effectiveness (PSE) for multiple antenna locations shows good agreement across the non-reverberant frequency regime, enabling fast, measurement-free SE prediction that is useful for shielded enclosure design and dense internal statistical sampling.

Keywords—simulation, reverberation chamber, non-reverberant, resonant, shielding effectiveness, plane-wave superposition, small enclosures.

I. Introduction

Shielding enclosures are widely used to control electromagnetic coupling into sensitive electronics, but their shielding effectiveness (SE) is not a single number. In the non-reverberant frequency range, where the enclosure is dominated by only a few discrete modes and the internal field is not statistically uniform [1], SE strongly depends on frequency, the enclosure and aperture geometry, internal loading, and the measurement point of the internal field [2].

A reverberation chamber (RC) provides a useful measurement environment for enclosure SE because it can generate an ensemble of field realizations by mechanical stirring, and RC based SE measurement methods are well established [3]. However, in the non-reverberant frequency range of a fully or partially loaded enclosure, practical measurement constraints become significant. Access to the enclosure interior is limited, placing probes can disturb the boundary conditions, and it is difficult to obtain dense spatial sampling throughout the enclosure volume while keeping the loading configuration unchanged [2], [3]. These limitations make it challenging to do the shielding measurement and investigating how SE varies across multiple internal measurement points and loading conditions using RC measurements alone.

To address these limitations, this paper presents and validates a plane-wave superposition (PWS) simulation based on a numerical approach that emulates an RC like excitation without explicitly modelling the full chamber and its stirrers which is likely to be computationally infeasible. First the Gauss-Legendre Quadrature (GLQ) method described in [4], [5] and the Lebedev method defined in [6] are compared. Both methods can be used to define a set of incident wave directions for the plane-wave illumination each having two orthogonal polarizations. The GLQ method is then combined with the PWS approach used in [1], [5], [7], [8] to generate a large ensemble of independent realizations from a finite set of full-wave simulations. Here, the main focus is the resonant (but not fully reverberant) region of the enclosure used in [2], [9] that covers a 300 MHz to 1 GHz frequency range.

This project has received funding from the European Union's EU Framework Program for Research and Innovation Europe Horizon (Grant Agreement No 101072881, for Doctoral Researcher Positions 1-4, 6-8 and 10-12) and UKRI (EP/X033481/1), for Doctoral Researcher Positions DR5 and DR9.

Section II provides detailed descriptions of the numerical modelling used in this study with the PWS technique, the methods for sampling the directions of illuminations, and the enclosure used in this study. Discussion of the measurement approach is provided in section III. The results of the proposed setup and RC measurements are analysed and discussed in Section IV. Conclusions are discussed in Section V.

II. Numerical Modelling

Simulating a physical RC in CST Microwave Studio [10] is computationally expensive, because modelling the full chamber volume together with mechanical stirrers is challenging in terms of memory and run time. Instead, an efficient PWS approach as detailed in [4], [5] was adopted that allows the simulation of a diffuse, statistically uniform field environment without modelling the chamber itself. This can be used to measure the SE of loaded enclosures in non-reverberant frequency range.

A key advantage of this setup is that it allows an unlimited number of internal measurement points that can be studied in statistical analysis. In a physical RC, especially shielding measurements, moving a probe inside a loaded enclosure in its non-reverberant frequency range would disturb boundary conditions and alter the field. In the simulation, multiple E- and H-field probes can be placed without probe loading effects and limitations that appears in physical RC measurement.

A. Plane-Wave Superposition (PWS)

A single plane-wave illumination in CST simulation has a fixed orientation and polarization, so the RC environment must be created through post processing. Following the techniques established in [1], [5], [7], [8], we utilize a superposition approach to imitate the RC and mechanical stirring effect.

In this approach, from the initial set of plane-wave simulations, a random subset (N) is selected. Then each wave in this subset is assigned a random phase, and the average of all plane-waves in this subset is taken to form one superposition. Mathematically, this superposition represents the angular spectrum components that, in a physical RC, would have travelled through different scattering paths before reaching the enclosure.

The main advantage of this approach is its flexibility. By resampling different subsets and phase combinations from the same original runs, we can generate a large number of independent realizations without running additional full-wave simulations. This ensures that the simulated environment maintains the same stochastic properties as a physical RC, all without the need for additional, time-consuming simulation runs.

B. Comparison of GLQ and Lebedev Methods

To simulate the RC environment in CST, the enclosure is illuminated by plane-waves with two orthogonal polarizations and incidence directions distributed over a spherical surface. Two angular sampling methods for generating these directions are compared here.

GLQ is a one dimensional rule for integrals on an interval that approximates with a weighted sum [4], [5]:

$$\int_{-1}^{1} f(x)dx \approx \sum_{i=1}^{n} \omega_i f(x_i) \tag{1}$$

where the points x_i are the roots of the nth Legendre polynomial and this choice makes the rule exact for polynomials up to degree $2n–1$. To use GLQ for directional integrals on a sphere, a product rule of $\mu = \cos\theta \in [-1,1]$ and a uniform rule in $\emptyset \in [0,2\pi]$ is needed. So, we have:

$$\int_{0}^{2\pi} \int_{-1}^{1} f(\mu,\emptyset)\, d\mu\, d\emptyset \approx \sum_{i=1}^{n} \sum_{j=1}^{M} \omega_i \left(\frac{2\pi}{M}\right) f\left(\mu_i,\emptyset_j\right) \tag{2}$$

Equation (2) creates rings of points at fixed θ that makes non-isotropic sampling points (Fig. 1). To overcome this limitation, the sampling points must be increased (increasing n and M). However, the Lebedev Quadrature [6] is built directly on the sphere surface:

$$\int_{S^2} f(\Omega) d\Omega \approx 4\pi \sum_{k=1}^{N} \omega_k f(\Omega_k) \tag{3}$$

here, the points Ω_k are arranged with octahedral symmetry and it is designed to integrate spherical harmonics up to a specified degree. This Lebedev grid, as it is shown in Fig. 1, tends to give a more uniform set of directions compared to GLQ.

In CST, each incident direction and polarization requires a separate full-wave run, so the main trade-off is the computational cost of this setup. References [4], [5] use the GLQ method to distribute plane-wave directions over the sphere, and [5] reports that 32 directions (Fig. 2), equivalent to 64 simulations when two orthogonal polarizations are included, are sufficient for statistical convergence using the Finite Integration Technique (FIT) in CST. The closest Lebedev set to this case is 38 directions (76 simulations with two polarizations).

Although Lebedev set tends to give a more genuinely isotropic sampling, as the directions are distributed more uniformly over the sphere rather than concentrating along a few constant latitude rings, it requires twelve additional full-wave runs in CST. Using the University of York facility, each run takes approximately 10 hours, making this increase substantial.

To compare the GLQ and Lebedev sampling methods, two simulation sets have been run in free space without any enclosure in place. One simulation set used the (θ, ϕ) directions generated by the Lebedev Quadrature and the other one used those generated by GLQ method.

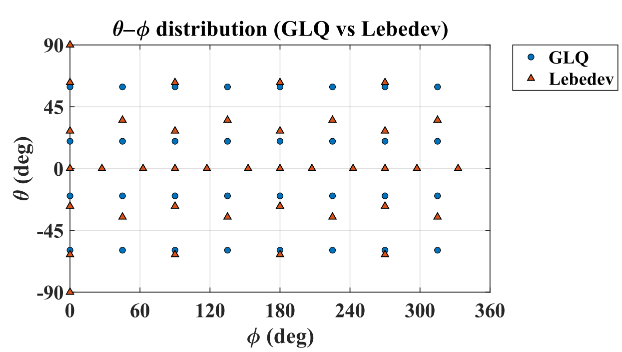

Fig. 1. 2D view of comparison between GLQ and Lebedev sampling points in θ − ϕ map. The GLQ points lie on constant-θ rings, whereas Lebedev points span multiple θ values, providing a more uniform distribution over the sphere.

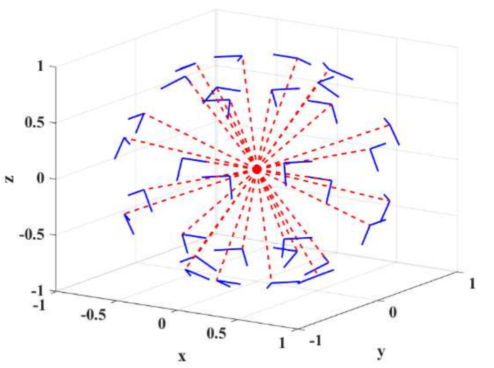

Fig. 2. The 32 sampling points (using GLQ method) as the angles of incidence distributed across the sphere considering the enclosure in the centre [5].

As noted in [2], in the non-reverberant frequency region the field inside an enclosure is not statistically uniform. Therefore, in the CST results, especially when analysing the E-field probes, the field cannot be treated as a single overall quantity with identical statistics in all directions. Instead, the three components of the electric field (E_x, E_y, and E_z) should be studied separately. Accordingly, this paper here analyses each field components individually.

A grid of 90 E-field probes (270 field samples when the x, y, and z components are considered) is defined to allow detailed analysis here. The E-field probes were placed uniformly with 100 mm spacing between neighbouring points in all directions. This probe layout was chosen deliberately to sample the full volume of the enclosure used in the later simulations, rather than focusing on a small region. With this spacing the field variation throughout the volume can be evaluated in a consistent and repeatable way.

In Fig. 3, the mean value (averaged over 100 PWS) is plotted for each probe location and field component in free space. To make the difference between the curves more obvious, for each probe the data are additionally smoothed by averaging over a 5 MHz window. The red curves correspond to Lebedev sampling, and the black curves correspond to GLQ.

The comparison makes the difference quite clear as the Lebedev sampling produces a more statistically uniform field distribution across directions than GLQ. With GLQ, the result shows a noticeable directional bias in the z-direction. Due to the specific plane-wave directions and how they are distributed on the sphere, the E_z component for GLQ is offset relative to E_x and E_y (Fig. 3). In this case, E_z from the GLQ method differs by roughly 1.2 dB compared to E_x and E_y. When we compare the two sampling methods directly, the difference between GLQ and Lebedev is around 0.4 dB for E_x and E_y, and about 1 dB for E_z.

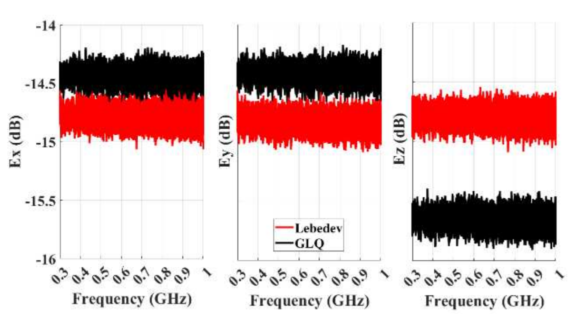

Fig. 3. Comparison of the E_x, E_y, and E_z components measured by the E-field probes in free space using the Lebedev and GLQ sampling methods in CST.

The Rician K-factor [11] is a practical way to describe how much of the received signal in a statistically uniform environment like an RC is unstirred versus stirred. The unstirred part behaves as a fixed, line of sight (LOS) contribution between the transmit and receive antennas, while the stirred part arrives after many reflections and changes as the chamber is perturbed (stirrer rotations or PWS).

For good statistical field behaviour, the unstirred contribution should be as small as possible [11]. Therefore, a low K-factor, indicates a well stirred environment, whereas a high K-factor suggests a stronger unstirred component remains. In terms of S-parameters (between the transmit and receive antennas in the RC measurement) and E-field, the K-factor can be computed by averaging over an ensemble of realizations (either stirrer rotations or PWS) using the (4) and (5) respectively:

$$\mathrm{K} = \frac{|\langle S_{21}\rangle|^2}{\langle |S_{21} - \langle S_{21}\rangle|^2\rangle} \quad (4)$$

$$\mathrm{K}^{\mathrm{i}} = \frac{\left|\langle E_{21}^{i}\rangle\right|^2}{\langle \left|E_{21}^{i} - \langle E_{21}^{i}\rangle\right|^2\rangle}\ ,\ i = x, y, z \quad (5)$$

where $\langle\ \rangle$ denotes averaging across realizations. The numerator of (4) and (5) represents the unstirred component obtained from the complex mean of S_{21} and E_{21}^{i} respectively, while the denominator captures the stirred component via the variance around that mean. For E-field probes, as defined in (5), the K-factor for each component is defined separately.

As it is shown in Fig. 4, calculating the K-factor for the PWS ensemble using the E-field probes in free space for both of the GLQ and Lebedev methods result in a value around –22 dB. This shows both of these methods provide comparable uniform environments for E-field probes.

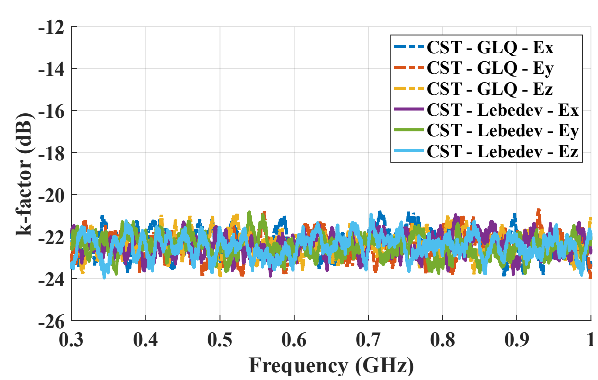

Fig. 4. Comparing the K-factor for the GLQ and Lebedev sets for E-field probes in CST.

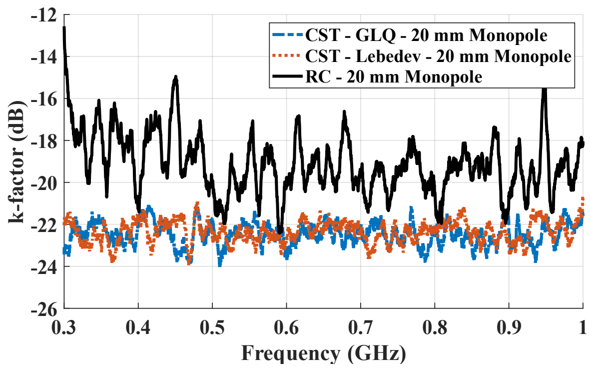

Fig. 5. Comparison of K-factor between the results of the CST setups and a real RC measurement for a 20 mm monopole on a reference plane (unshielded case).

Fig. 5 compares the K-factor for an unshielded 20 mm monopole mounted on a metal reference plane, using both CST and RC measurements. In the RC, the K-factor falls in the range of about –15 dB to –22 dB, while in CST it is around –22 dB for both the GLQ and Lebedev direction sets. Overall, this level of agreement suggests that the CST excitation used here provides a good reverberation like environment for the study.

In practice, both GLQ and Lebedev show similar overall performance, so there is a trade-off in which Lebedev provides better directional uniformity but requires twelve additional simulations compared with GLQ. Because the differences observed here are small, the remaining simulations were performed using GLQ to reduce computational cost while keeping the impact on the results minimal.

C. The Enclosure and Contents

For the simulation in CST, the dimensions of the physical enclosure used in [2], [9] were replicated, including an aperture of 140 mm × 40 mm (Fig. 6a). Here, the brass material with conductivity of 1.59×10^7 S/m, and thickness of 1.5 mm was used. To minimise the mesh size, mechanical details such as joints and seams were omitted. This simplification avoids the very fine mesh required for specific details and gaps and allows the study to focus on the internal resonant behaviour and the impact of the enclosure contents.

For the enclosure contents, the CST model uses the radiation absorbent material representative contents (RAM ReCo) described in [5] as a computationally efficient surrogate for the transmission line representative contents (TL ReCos) used in measurements. The ground plane was modelled as a perfect electric conductor (PEC), and eight LS22 RAM absorbers were modelled as lossy dielectric blocks, each with dimensions of 9.5 mm × 40 mm × 22.5 mm (Fig. 6b). The absorbers were placed on the PEC plane with a spacing of 25 mm along the length and 38 mm across the width. In terms of absorption cross section (ACS), this RAM ReCo provides a good match to the TL ReCos used in [2], [5], [9] (Fig. 6c).

III. Measurement Approach

In previous work [2], it was shown that when looking at EM shielding behaviour across different physical environments, the non-reverberant frequency range includes the resonant and the

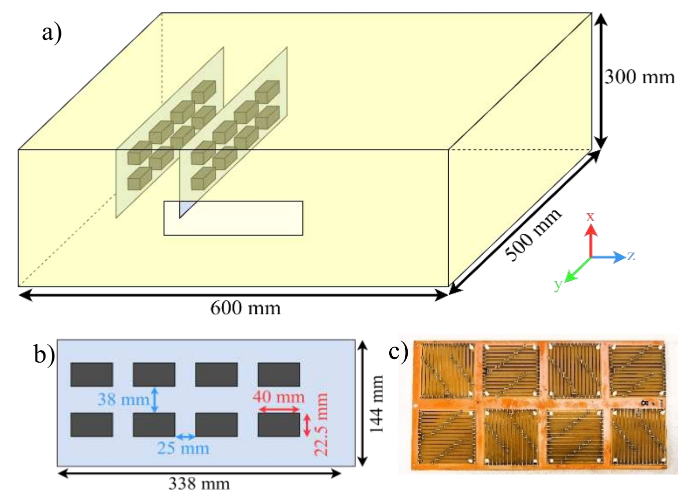

Fig. 6. a) The brass enclosure with two internal LS22 RAM ReCos modelled in CST, b) The LS22 RAM ReCo dimensions used as a content inside the enclosure in CST, c) The TL ReCo used in physical RC measurements.

transition regions, where the transition region gradually connects the resonant region to the reverberant range.

In this paper, the frequency range of the interest is 300 MHz to 1 GHz that covers the resonant region of the enclosure (with the fundamental TE_{011} mode at 390 MHz). This frequency range is where the physical geometry of this enclosure, along with its aperture, internal components, and their placement have a very strong influence on the internal field structure and shielding behaviour.

A. Physical RC Measurement Set-up

The shielding measurements for the enclosure, loaded with TL ReCos, were performed in the mechanically stirred RC located in the University of York laboratory using the method described in [3]. The dimension of this RC is 4.7 m × 3 m × 2.37 m. A mechanical stirrer with one hundred positions per full rotation is used to have mode stirring within the RC.

A vector network analyser (VNA) was used to measure the S-parameters between the transmit (Tx) antenna inside the RC and each receive (Rx) antenna. The VNA was set to an output power of 10 dBm with an intermediate frequency bandwidth (IFBW) of 10 kHz. Measurements were taken both without shielding (reference case) and with the enclosure in place (shielded case).

Over this frequency band, the measured response of the enclosure is dominated by discrete resonances, so a fine frequency sweep was needed to resolve the resonant peaks relative to their Q bandwidths. For that reason, 20001 frequency points were measured, corresponding to a 35 kHz frequency step.

To make the RC measurements comparable with the CST simulations, we used TL ReCos (Fig. 6c) as the enclosure contents [2]. As mentioned before, these TL ReCos were chosen because their ACS is similar to the RAM ReCos modelled in CST [5]. Each TL ReCo is made up of sixteen unit cells. Every unit cell contains 29 resistively loaded transmission line tracks. The unit cells are arranged evenly, with eight on each side of a double-sided carrier PCB. A single basic TL ReCo measures 280 mm × 145 mm, as shown in Fig. 6c.

In this paper, for the enclosure the same antenna placement as in [2] is used. However, two of the three 20 mm monopoles mounted on orthogonal walls were kept and the third one (on the 500 mm × 600 mm wall) was replaced with an 80 mm monopole to improve impedance matching and coupling compared with the 20 mm monopole over the frequency region of interest. The instrumented TL ReCo, with four additional monopoles (monopole A-D) mounted on one of the TL ReCos, were also kept. These monopoles were installed on one side of the instrumented TL ReCo and connected through the back wall of the enclosure using coaxial cables.

The physical enclosure was loaded with two TL ReCos (two RAM ReCos in the CST model), spaced 80 mm apart. One was a basic TL ReCo, and one was an instrumented TL ReCo carrying four monopoles.

B. *Simulation Set-up*

In the CST simulations, in addition to monopoles on the RAM ReCos and monopoles on the walls, the same grid of 90 E-field probes (270 field samples) is also included to allow detailed analysis that is not presented here.

Since the focus of this study is on modelling an RC environment in CST, running full-wave simulations with this setup allows us to capture the field behaviour across different measurement points and under different loading conditions.

IV. Results and Discussions

A. *Comparison of point SE Results for CST and RC Approaches*

To assess how reliable the CST approach is, here the point SE (defined in [12]) is used for each field sample (monopole or probe):

$$\mathrm{SE_n} = 10\log_{10}\left|\frac{E^n_{ref}}{E^n_{sh}}\right|^2 \quad (6)$$

where $\mathrm{SE_n}$ is the SE value at stirrer position *n* (or *n*th PWS in CST) and E^n_{ref} and E^n_{sh} are the fields measured without the shield and with the shield installed respectively. The averaged point SE (over 100 stirrer positions or PWS) obtained from both the CST PWS approach and the physical RC is compared. In both configurations, the overall averaged point SE behaviour is comparable between the model and measurement.

As it is shown in Fig. 7 and Fig. 8, at lower frequencies the curves are relatively smooth and in good agreement. However, at higher frequencies the response becomes more structured as the modal density increases and resonances begin to overlap. Importantly, the main resonance locations line up well between CST and RC, which suggests that the CST model captures the dominant cavity behaviour.

The analytically predicted resonant frequencies for the empty closed enclosure (vertical dotted lines in Fig. 7 and Fig. 8) are included, while noting that introducing the rectangular aperture and adding internal contents shifted these resonant frequencies [13].

For the monopoles mounted on the enclosure walls, CST simulations and the RC measurements show very similar averaged point SE patterns across the full measurement band (Fig. 7). The deepest averaged point SE minima occur at the same frequencies for each monopole, and the relative ordering between the monopole curves is also consistent. The remaining differences are mainly in the depth of the narrow dips, which is expected because small practical details, such as electrical contacts, joints, bolts, and differences in the internal loading and contents design, can change the coupling and therefore the dip depth even when the resonance frequency matches.

For the instrumented TL ReCo monopoles (monopoles A-D), the agreement is again strong in terms of resonance positions and the overall trend between the simulation and the measurement, although the spread between different monopoles becomes more noticeable (Fig. 8).

Overall, the CST results reproduce the main averaged point SE behaviour observed in the RC measurements, supporting the CST PWS approach as a practical alternative to explicitly modelling the full RC. This will allow us to have more measurement points, as mentioned before, to investigate the statistical behaviour of the enclosure within these points with different loadings without having the limitations of using RC approach in resonant and non-reverberant frequency range.

V. Conclusion

This work compared an efficient simulated based approach with the RC measurements in the non-reverberant frequency range using plane-wave illumination and PWS method. Two

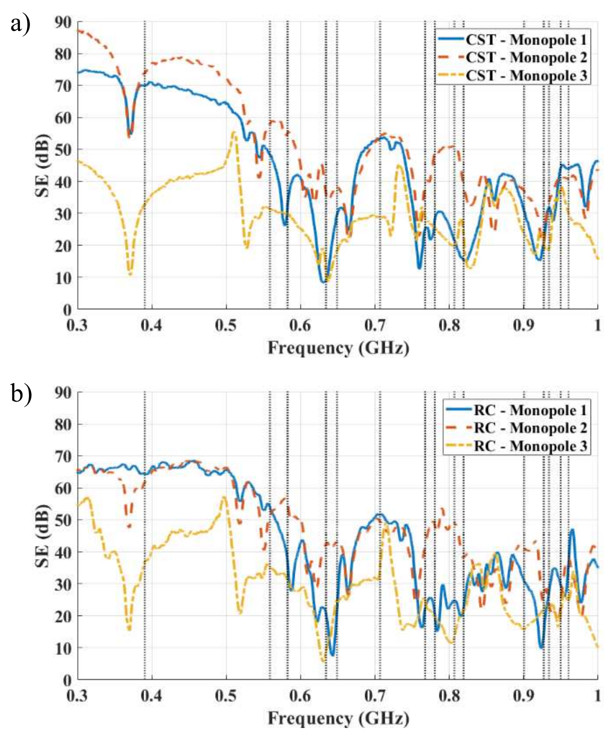

Fig. 7. The averaged point SE comparison for the Monopoles 1-3 mounted on the walls, a) CST results using the PWS approach and GLQ sampling method; b) measured results in the RC. Vertical dotted lines mark the resonant frequencies of empty closed enclosure used for reference.

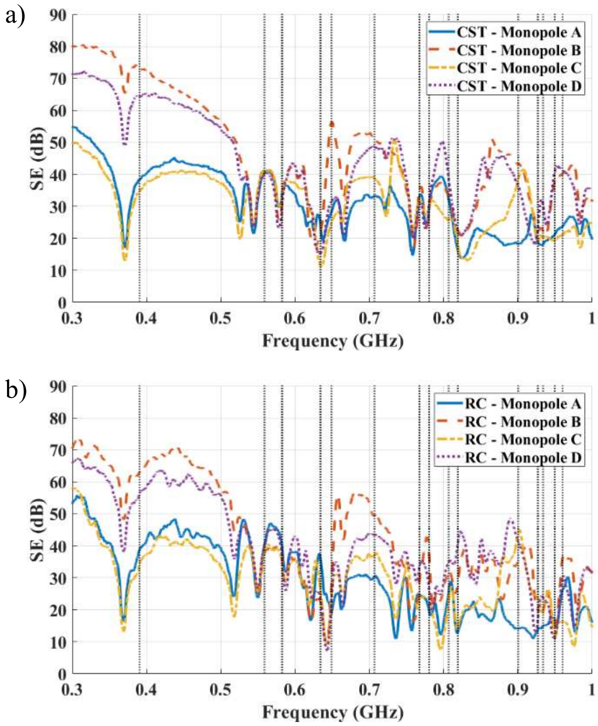

Fig. 8. The averaged point SE comparison for the Monopoles A-D placed on contents, a) CST results using the PWS approach and GLQ sampling method (Monopoles A-D on RAM ReCo); b) measured results in the RC (Monopoles A-D on instrumented TL ReCo). Vertical dotted lines mark the resonant frequencies of empty closed enclosure used for reference.

sampling method, GLQ and Lebedev direction sets, are evaluated and the GLQ is selected as a practical sampling method in this approach as it requires twelve fewer simulations while showing similar performance. Validation against the RC measurements showed that the CST and PWS excitation produces a statistically uniform environment for the purposes of this study. The K-factor levels, that were obtained numerically, were comparable to the measured RC result.

When comparing averaged point SE, the CST model reproduced the dominant measured behaviour across 300 MHz to 1 GHz, including consistent resonance locations for both wall mounted monopoles and instrumented TL ReCo monopoles.

The main discrepancies were observed in the depth of narrow resonant minima, which is expected in high-Q conditions where small changes in coupling such as aperture details, contact quality, cable routing, and differences between simulated and measured loading can significantly affect the measured dip magnitude even when resonance frequencies align.

Overall, the agreement between CST and RC results supports the CST PWS approach as a practical alternative to explicitly modelling the full RC. This is useful for designers of shielded enclosures because it enables fast, accurate prediction of resonant and non-reverberant SE performance without relying on prototype measurements, supporting earlier design decisions and faster iteration.

While this paper focused on validating the method through averaged point SE comparisons, the same framework naturally enables dense internal sampling across the enclosure volume and systematic studies of loading placement and orientation. These statistical, volume wide investigations are left as the next step.

REFERENCES

[1] D. A. Hill, "Plane wave integral representation for fields in reverberation chambers," *IEEE Transactions on Electromagnetic Compatibility*, vol. 40, no. 3, pp. 209–217, Aug. 1998, doi: 10.1109/15.709418.

[2] A. G. Raef, A. C. Marvin, S. J. Bale, M. P. Robinson, and J. F. Dawson, "Shielding Effectiveness of Enclosures: Characterising the Transition from Reverberant to Resonant Behavior," in *2025 International Symposium on Electromagnetic Compatibility – EMC Europe*, Sep. 2025, pp. 338–343. doi: 10.1109/EMCEurope61644.2025.11176219.

[3] *IEEE Standard Method for Measuring the Shielding Effectiveness of Enclosures and Boxes Having all Dimensions between 0.1 m and 2 m*. doi: 10.1109/IEEESTD.2014.6712029.

[4] H. Xie, J. F. Dawson, J. Yan, A. C. Marvin, and M. P. Robinson, "Numerical and Analytical Analysis of Stochastic Electromagnetic Fields Coupling to a Printed Circuit Board Trace," *IEEE Transactions on Electromagnetic Compatibility*, vol. 62, no. 4, pp. 1128–1135, Aug. 2020, doi: 10.1109/TEMC.2019.2954303.

[5] I. D. Flintoft *et al.*, "Representative Contents Design for Shielding Enclosure Qualification From 2 to 20 GHz," *IEEE Trans. Electromagn. Compat.*, vol. 60, no. 1, pp. 173–181, Feb. 2018, doi: 10.1109/TEMC.2017.2702595.

[6] V. I. Lebedev and D. N. Laikov, "A QUADRATURE FORMULA FOR THE SPHERE OF THE 131ST ALGEBRAIC ORDER OF ACCURACY," *Doklady Mathematics*, vol. 59, pp. 477–481, 1999.

[7] F. Moglie and A. P. Pastore, "FDTD analysis of plane wave superposition to simulate susceptibility tests in reverberation chambers," *IEEE Transactions on Electromagnetic Compatibility*, vol. 48, no. 1, pp. 195–202, Feb. 2006, doi: 10.1109/TEMC.2006.870793.

[8] D. Fedeli, G. Gradoni, V. M. Primiani, and F. Moglie, "Accurate Analysis of Reverberation Field Penetration Into an Equipment-Level Enclosure," *IEEE Transactions on Electromagnetic Compatibility*, vol. 51, no. 2, pp. 170–180, May 2009, doi: 10.1109/TEMC.2009.2013456.

[9] A. Ghaffarlouy Raef, A. C. Marvin, S. J. Bale, M. P. Robinson, and J. F. Dawson, "Enhanced Prediction and Measurement of the Shielding Effectiveness of Reverberant Equipment Enclosures," in *2024 International Symposium on Electromagnetic Compatibility – EMC Europe*, Sep. 2024, pp. 595–600. doi: 10.1109/EMCEurope59828.2024.10722550.

[10] *Microwave Studio, Computer Simulation Technology (CST). 2025. [Online]. Available: https://www.cst.com*.

[11] C. Lemoine, E. Amador, and P. Besnier, "On the K -Factor Estimation for Rician Channel Simulated in Reverberation Chamber," *IEEE Transactions on Antennas and Propagation*, vol. 59, no. 3, pp. 1003–1012, Mar. 2011, doi: 10.1109/TAP.2010.2103003.

[12] A. C. Marvin, J. F. Dawson, H. Xie, L. Dawson, and A. Venkateshaiah, "An Experimental Study of the Variability of the Shielding Effectiveness of Circuit Board Shields," in *2020 International Symposium on Electromagnetic Compatibility - EMC EUROPE*, Rome, Italy: IEEE, Sep. 2020, pp. 1–5. doi: 10.1109/EMCEUROPE48519.2020.9245741.

[13] M. P. Robinson *et al.*, "Analytical formulation for the shielding effectiveness of enclosures with apertures," *IEEE Trans. Electromagn. Compat.*, vol. 40, no. 3, pp. 240–248, Aug. 1998, doi: 10.1109/15.709422.